arXiv:1411.0025v1 [cond-mat.mes-hall] 31 Oct 2014

Optically Active Quantum Dots in Monolayer WSe_2

Ajit Srivastava[1*], Meinrad Sidler[1*], Adrien V. Allain[2],

Dominik S. Lembke[2], Andras Kis[2], and A. Imamoğlu[1]

[1] *Institute of Quantum Electronics, ETH Zurich, CH-8093 Zurich, Switzerland and*

[2] *Electrical Engineering Institute, Ecole Polytechnique*

Federale de Lausanne (EPFL), CH-1015 Zurich, Switzerland.

*Correspondence to: imamoglu@phys.ethz.ch, sriva@phys.ethz.ch

Semiconductor quantum dots have emerged as promising candidates for implementation of quantum information processing since they allow for a quantum interface between stationary spin qubits and propagating single photons [1–3]. In the meanwhile, transition metal dichalcogenide (TMD) monolayers have moved to the forefront of solid-state research due to their unique band structure featuring a large band gap with degenerate valleys and non-zero Berry curvature [4]. Here we report the observation of quantum dots in monolayer tungsten-diselenide with an energy that is 20 to 100 meV lower than that of two dimensional excitons. Photon antibunching in second-order photon correlations unequivocally demonstrates the zero-dimensional anharmonic nature of these quantum emitters. The strong anisotropic magnetic response of the spatially localized emission peaks strongly indicates that radiative recombination stems from localized excitons that inherit their electronic properties from the host TMD. The large ~ 1 meV zero-field splitting shows that the quantum dots have singlet ground states and an anisotropic confinement most likely induced by impurities or defects in the host TMD. Electrical control in van der Waals heterostructures [5] and robust spin-valley degree of freedom [6] render TMD quantum dots promising for quantum information processing.

Main Text

Advances in semiconductor based quantum information processing have been made on two disjoint fronts: while optically active self-assembled quantum dots (QD) with deep electron and hole confinement allow for the realization of highly efficient single-photon sources [7], all-optical manip-

ulation of confined spins [8, 9] and a spin-photon quantum interface [3, 10], the random nature of their growth seems to be the biggest hinderance towards their use in scalable quantum information processing. In contrast, electrically-defined single [11] or double QDs [12] hosting one or two excess electrons have been shown to exhibit long spin coherence times together with a clear path towards integrated scalable devices. However, weaker confinement has precluded the possibility to reliably transfer quantum information from spins to photons in these systems. QDs in monolayer TMDs have the potential to combine the desirable features of both optically active and electrically-defined QDs: while we report tungsten-diselenide (WSe_2) QDs that appear due to uncontrolled impurity or defect induced traps, the two dimensional (2D) nature of these materials makes it easier to electrically control the local potentials on a scale of few tens of nanometers. More importantly, strong electron-hole binding in TMDs suggest that it would be possible to obtain a quantized optical excitation spectrum due to trapping of excitons or trions in large electric field gradients induced by external gates [13].

The samples studied in our experiments were obtained by mechanical exfoliation from WSe_2 synthetic crystals onto heavily doped silicon substrates with 285 nm SiO_2 layer on top [14, 15]. Monolayer flakes were identified using their optical contrast. Polarisation-resolved photoluminescence (PL) and resonant white-light reflection spectroscopy were performed using a home-built confocal microscope setup placed in a liquid helium bath cryostat. The sample temperature was 4.2 K and the excitation source was a helium-neon (HeNe) laser at 632.8 nm or a tunable continuous-wave (cw) Ti:Sapphire laser. The spot size for excitation wavelength was $\sim 2\mu$m.

Figure 1a (left panel) shows photoluminescence (PL) spectra of a monolayer flake (flake0) of WSe_2 not showing sharp emission peaks at two different excitation laser powers (P_{exc}). The spectra clearly shows two high energy peaks: exciton (X^0) emission at 708 nm, charged exciton (trion) emission (X^-) at around 722 nm at high P_{exc}. These assignments are in accordance with previous reports of PL from monolayer WSe2 [16]. The third feature of the spectra is the broad emission to the lower energy side of the trion peak, that has been previously attributed to impurity/defect trapped excitons in WSe_2 and other TMDs [17]. At low P_{exc}, X^0 and X^- peaks are too weak to be detected while the impurity band peak can still be seen, suggesting starkly different power-dependence of the impurity band as compared to X^0 and X^- peaks. A detailed power dependence of X^0, X^- and the impurity band shown in Figure 1a (right panel) confirms this claim - while the integrated PL intensity of X^0 and X^- peaks shows linear dependence up to the highest ($P_{exc} \sim$

320 μW), that of the impurity band exhibits saturation behaviour (sub-linear dependence) even at powers as low as $\sim$ 100 nW. We do not observe any broadening of the X^0 and X^- peak even at the highest P_{exc} while the spectral features of the impurity band change significantly with incident laser power (see Supplementary Fig. S1).

This type of saturation behavior at relatively low powers compared to free excitons is indeed consistent with PL that stems from defects and impurities which act as two-level emitters. It is well known from optical investigation of quantum well structures in III-V semiconductors that in low quality samples with a high defect or impurity density, the PL is dominated by red-shifted emission from these localized state. This is a consequence of the fact that optically generated excitons relax by phonon emission into the localized states, quenching the delocalized exciton emission.

Figure 1b shows PL spectra for another WSe_2 flake (flake1) where the impurity band is comprised of sharp emission peaks which become prominent at lower P_{exc} and finally for $P_{exc} \leq 1\mu$W, only sharp peaks are visible while the X^0 peak becomes too weak to be detected. Figure 1c (right panel) shows a spatial map of integrated PL intensity for X^0 (area enclosed by the black contour in Figure 1c) and two different sharp emission peaks (left panel) on flake1 obtained by raster scanning the sample with piezoelectric positioners. The sharp emission peaks are seen to be spatially localised such that PL spectra at energies lower than X^- emission appear strikingly different at different locations on the flake. High resolution PL spectrum of the two sharp peaks, labeled QD1F1 and QD2F1 are obtained with $P_{exc} < 1$ μW and exhibit extremely narrow linewidths of less than 120 μeV, possibly limited by spectral diffusion of the emission peak as discussed below. We rule out Raman scattering as the origin of the sharp features since changing the energy of the incident laser does not result in any corresponding shift in the emission energy. It is interesting to note that we observe strong PL from a region (coloured red in Figure 1c) where the exciton emission is more than an order of magnitude weaker than its maximum value. We also measured differential reflectance of the flake using a broadband white light source which shows a clear peak only for X^0 [18].

To prove that the sharp emission peaks originate from localized excitons with an anharmonic spectrum, we measure the photon correlation function $g^2(\tau)$ using a Hanbury-Brown-Twiss (HBT) setup with two single photon counting avalanche photodiodes (APDs). Since $g^2(\tau = 0)$ gives the likelihood for detecting two photons simultaneously, an ideal single zero-dimensional (0D) emitter with uncorrelated background contribution gives $g^2(0) = 0$. In general, a measured value

of $g^2(0) < 0.5$ unequivocally proves that the source of emission originates predominantly from a single anharmonic emitter – a quantum dot (QD). Figure 2a shows the $g^2(\tau)$ measurement results for QD1F1 and QD2F1, yielding $g^2(0) = 0.18 \pm 0.02$ and $g^2(0) = 0.20 \pm 0.02$, respectively. We therefore conclude that the sharp peaks are indeed associated with QD PL. Figure 2b shows the PL lifetime of QDs QD1F1 and QD3F1 on flake1 measured by exciting with a $\sim$ 5 ps pulsed Ti:Sapphire laser tuned into resonance with X^0 transition and sending the spectrally filtered output around the QD wavelength to a single-photon-counting APD with a timing resolution of $\sim$ 350 ps. The measured long lifetime of few nanoseconds is consistent with behavior shown by typical semiconductor quantum dots. In contrast, the exciton lifetime in MoS_2 is reported to be about 4 ps [19] and is determined predominantly by non-radiative decay.

It is well known that 0D emitters in solids typically exhibit spectral diffusion [20], blinking and in some cases photo-bleaching. To determine if WSe_2 QDs also exhibit these properties that strongly limit their applications, we record the single photon detection events for QD1F1 using a single-photon counting APD with a dead time of $\sim$ 200 ns at a total photon counting rate of $\sim$ 13 kHz. We then use this data to obtain the waiting time distribution $W(\tau)$ for $\tau \geq 10\mu$s. Figure 3a shows that $W(\tau)$ can be fitted by a single exponential where the decay time is given by $\tau_{det} = (\Gamma\eta)^{-1} \sim 77$ μs, in excellent agreement with the measured photon counting rate. Here Γ is the spontaneous emission rate and η is the detection efficiency. This observation shows that there is no blinking for timescales longer than τ_{det}: in the event of intensity intermittency or blinking one expects the intensity to exhibit bright and dark states between which the system switches randomly. If this switching takes place on a time-scale $\tau_{blink} > \tau_{det}$, then $W(\tau)$ should have an additional decay on a timescale determined by τ_{blink} [21]. The absence of bunching on timescales ≤ 1 μs in $g^2(\tau)$ measurements (not shown) in turn rule out blinking on such short timescales. Finally, we emphasize that blinking statistics in most QDs is known from prior studies to be non-Poissonian, exhibiting power-law tails in waiting time distribution [20]. In the absence of any such deviation from an exponential decay, we tentatively conclude that there is no significant blinking in the QDs studied here.

We emphasize that there is no obvious degradation of PL intensity up to hundreds of μWs of incident HeNe laser power, way above the linear response regime of QDs. The QD PL also survived several cycles of warm-up to room temperature and cool-down to 4.2 K; these observations allow us to conclude that the QDs do not photo-bleach. However, spectral diffusion of the emission peak

with excursion range of a few hundred μeV is observed in almost all QDs but with varying strength. Most QDs exhibit small spectral diffusion with range $\pm 200\mu$eV which cannot be resolved using a low-resolution spectrometer (Fig. 3b). On the other hand, we observed that some QDs exhibited large spectral diffusion of range ± 0.5 meV (Fig. 3c); such strong spectral diffusion, probably arising from charge fluctuations in the environment of the QDs, could last up to minutes before the peak energy is stable again.

Having established that the sharp emission peaks stem from optically active QDs, we focus on demonstrating that the QDs inherit their electronic properties, such as the valley degree of freedom, from WSe_2. A priori, it is not clear whether the QD confinement strongly mixes the two valleys. Below we provide evidence that there is no valley hybridization in TMD QDs studied here.

A first test in this regard is provided by photoluminescence-excitation (PLE) measurement where we tune an excitation laser across the free exciton and trion peaks and monitor the PL intensity of QDs. As we demonstrate in Fig. S2 (see Supplementary), we observe an overall enhancement in PL for most QDs suggesting efficient relaxation from free excitons to QD states. Remarkably, for all QDs on which PLE was performed, there is a sharp cut-off for excitation laser energy below which the PL signal drops drastically. As PLE probes the absorption spectra of the emitter, such a cut-off in laser energy could mark the onset of continuum states of the QD below which only sharp discrete states could exist.

To demonstrate the existence of a valley degree of freedom for the observed QDs, we perform polarisation-resolved magneto-optical spectroscopy with magnetic field (B-field) both perpendicular (Faraday geometry) and parallel (Voigt geometry) to the flake. It has been recently reported that only in the presence of a magnetic field perpendicular to the TMD flake, exciton and trion emission peaks split into two circularly polarised peaks of opposite helicities due to the lifting of valley degeneracy [18]. This strongly anisotropic magnetic response was attributed to two-dimensional electronic structure of TMDs. Magnetic field dependence of PL obtained by a linearly polarized excitation laser and detected in circularly-polarized basis in Faraday geometry is shown in Figure 4a (left panel): two split peaks are observed even at zero B-field with the splitting increasing with B-field. Most notably, no clear splitting is observed in the Voigt geometry just like in the case of exciton and trion (Fig.4a, right panel). The split peaks are circularly polarized with opposite helicities at finite B-field which reverse upon reversing the direction of B-field confirming that the peaks arise from the same QD (Fig. 4b). These observations strongly suggest that the QDs inherit

their electronic structure from the host TMD and are very likely to be excitons trapped in shallow defect or impurity potentials. Our findings also lend support to the recent prediction that valley hybridization is absent in TMD QDs, preserving the valley physics of 2D bulk [22].

As the splitting between the peaks increases at higher fields, the higher energy peak decreases in intensity. This is expected if there is efficient thermalization between the two levels before recombination as PL signal from a level is proportional to its occupancy. Although in most zero-dimensional systems, such a thermalization is highly inefficient, finite carrier density in TMDs could, in principle, enhance thermalization.

The observed zero-field splitting of about 700 μeV possibly originates from electron-hole exchange interaction of a neutral exciton trapped in an asymmetric confining potential, as is commonly observed in self-assembled InAs/GaAs quantum dots [23]. It could also arise if the exciton is bound to an ionized donor as no electron-hole exchange interaction is present when the exciton is bound to a neutral donor with a spin-1/2 ground-state. It is noteworthy that this zero-field splitting in TMD QDs is almost 50 times larger than that in InAs/GaAs self-assembled quantum dots [23], consistent with the strong Coulomb interactions in monolayer TMDs.

The splitting between the two peaks is plotted against B-field in Figure 4c and fit to a hyperbolic dispersion $E(B) = \sqrt{\mu^2 B^2 + \delta_0^2}$ expected for exchange-mixed circularly polarized resonances. We obtain $|\delta_0|$ between 650 to 850 μeV and μ between 7.5 to 10.9 μ_B (Bohr magneton) after fitting splitting data for several different QDs in two different flakes (see Fig. S3, supplementary). This measured magnetic moment of QD exciton is significantly larger than that of a free exciton, ~ 4 μ_B and a trion ~ 5.5 to 6 μ_B in WSe_2 [18].

An earlier study on defect activated PL in TMDs concluded that the impurity band emission arises from excitons trapped in anion vacancies [17] which could also be the origin of QDs studied here. In addition, recent high-resolution transmission electron microscopy (TEM) studies have revealed the presence of line defects and island-like domains within single MoS_2 layer [24]; it is plausible that such defects lead to exciton localization. Finally we remark that we observed strong emission from individual QDs in two flakes while most other flakes showed behaviour similar to flake0 presumably due to a much higher density of QDs leading to a formation of impurity band.

QDs in TMDs are likely to have very favorable properties for applications in quantum information processing [25]. Since we have established that quantum confinement does not lead to valley hybridization, a qubit defined using the two lowest energy states of an excess QD electron could

be classified as a spin-valley qubit. Given that the spin and valley degrees of freedom are strongly correlated due to large spin-orbit interaction, any decoherence mechanism that couples only to spin or to valley will remain ineffective. Unlike GaAs, the dominant isotopes of most TMDs are nuclear-spin free, rendering intrinsic hyperfine decoherence to be weak. An open fundamental question motivated by our work is the origin of the anomalously large g-factor of TMD QDs. Understanding the nature of quantum confinement would provide insights for engineering QDs within a monolayer.

---

[1] DiVincenzo, D. P., The Physical Implementation of Quantum Computation. *Fortschr. Phys.* 48, 771-783 (2000).

[2] Imamoğlu, A. *et al.* Quantum Information Processing Using Quantum Dot Spins and Cavity QED. *Phys. Rev. Lett.* 83, 4204 (1999).

[3] Gao, W.-B., Fallahi, P., Togan, E., Miguel-Sanchez, J. & Imamoğlu, A. Observation of entanglement between a quantum dot spin and a single photon. *Nature* 491, 426-430 (2012).

[4] Xu, X., Wang, Y., Di, X., Heinz, T. F., Spins and Pseudospins in layered transition metal dichalcogenides. *Nat. Phys.* 10, 343-350 (2014).

[5] Lee, C.-H. *et al.* Atomically thin p-n junctions with van der Waals heterointerfaces. *Nat. Nanotech.* 9, 676-681 (2014).

[6] Xiao, D., Liu, G.-B., Feng, W., Xu, X. & Yao, W., Coupled Spin and Valley Physics in Monolayers of MoS2 and Other Group-VI Dichalcogenides. *Phys. Rev. Lett.* **108**, 196802 (2012).

[7] Dousse, A. *et al.* Ultrabright source of entangled photon pairs. *Nature* 466, 217-220 (2010).

[8] Berezovsky, J., Mikkelsen, M. H., Stoltz, N. G., Coldren, L. A. & Awschalom, D. D., Picosecond Coherent Optical Manipulation of a Single Electron Spin in a Quantum Dot *Science* 320, 349-352 (2008).

[9] Press, D., Ladd, T. D., Zhang, B. & Yamamoto, Y., Complete quantum control of a single quantum dot spin using ultrafast optical pulses. *Nature* 456, 218-221 (2008).

[10] De Greve, K. *et al.* Quantum-dot spin-photon entanglement via frequency downconversion to telecom wavelength. *Nature* 491, 421-425 (2012).

[11] Elzerman, J. M. *et al.* Single-shot read-out of an individual electron spin in a quantum dot. *Nature* 430, 431-435 (2004).

[12] Petta, J. R. *et al.* Coherent Manipulation of Coupled Electron Spins in Semiconductor Quantum Dots *Science* 309, 2180-2184 (2005).

[13] Wilson-Rae, I., Galland, C., Zwerger, W. & Imamoglu, A. Exciton-assisted optomechanics with suspended carbon nanotubes. *New J. Phys.* 14, 115003 (2012).

[14] Novoselov, K. S. *et al.* Two-dimensional atomic crystals. *Proc. Natl Acad. Sci. USA* 102, 10451-10453 (2005).

[15] Radisavljevic, B., Radenovic, A., Brivio, J., Giacometti, V. & Kis, A., Single-layer MoS2 transistors. *Nat. Nanotech.* 6, 147-150 (2011).

[16] Jones, A. M. *et al.* Optical Generation of Excitonic Valley Coherence in Monolayer WSe_2. *Nat. Nanotech.* 8, 896-869 (2013).

[17] Tongay, S., *et al.* Defects activated photoluminescence in two-dimensional semiconductors: interplay between bound, charged, and free excitons. *Sci. Rep.* 3, 2657 (2013).

[18] Srivastava, A. *et al.* Valley Zeeman Effect in Elementary Optical Excitations of a Monolayer WSe_2. *arXiv:1407.2624v1.*

[19] Lagarde, D. *et al.* Carrier and Polarization Dynamics in Monolayer MoS_2. *Phys. Rev. Lett.* 112, 047401 (2014).

[20] Frantsuzov, P., Kuno, M., Janko, B. & Marcus, R. A., Universal emission intermittency in quantum dots, nanorods and nanowires. *Nat. Phys.* 4, 519-522 (2008).

[21] Delteil, A., Gao, W.-B., Fallahi, P., Miguel-Sanchez, J. & Imamoğlu, A. Observation of Quantum Jumps of a Single Quantum Dot Spin Using Submicrosecond Single-Shot Optical Readout. *Phys. Rev. Lett.* 112, 116802 (2014).

[22] Liu, G.-B., Pang, H., Yao, Y. & Yao, W., Intervalley coupling by quantum dot confinement potentials in monolayer transition metal dichalcogenides. *New J. Phys.* 16, 105011 (2014).

[23] Gammon, D., Snow, E. S., Shanabrook, B. V., Katzer, D. S. & Park, D., Homogeneous Linewidths in the Optical Spectrum of a Single Gallium Arsenide Quantum Dot. *Science* 273, 87-90 (1996).

[24] Enyashin, A. N., Bar-Sadan, M., Houben, L. & Seifert, G., Line Defects in Molybdenum Disulfide Layers *J. Phys. Chem. C* 117, 10842 (2013).

[25] Kormányos, A., Zólyomi, V., Drummond, N. D. & Burkard, G., Spin-Orbit Coupling, Quantum Dots, and Qubits in Monolayer Transition Metal Dichalcogenides. *Phys. Rev. X* 4, 011034 (2014).

Acknowledgments This work is supported by NCCR Quantum Science and Technology (NCCR QSIT), research instrument of the Swiss National Science Foundation (SNSF)

Figure 1: Photoluminescence of monolayer WSe_2 flakes a, (Left panel) Low temperature (4.2 K) photoluminescence (PL) spectra of a monolayer flake (flake0) not showing sharp peaks in emission at two different powers of incident laser (Helium-neon, 632.8 nm). Vastly different power dependence is observed for the exciton (X^0), trion (X^-) peaks and the broad feature (impurity band) at longer wavelengths. (Right panel) Detailed laser power dependence shows linear behaviour of the integrated PL intensity for X^0 (blue circles) and X^- (green diamonds) peaks whereas the impurity band (red squares) PL has sub-linear dependence. **b,** Low temperature PL spectra of a monolayer flake (flake1) showing sharp emission lines at high (low) laser power is plotted in the left (right) panel. X^0 peak is too weak to be detected at low power whereas the sharp emission peaks show saturation behaviour similar to the impurity band PL in Figure 1a. **c,** (Right panel) A spatial map of PL from flake1 showing localised emission of the sharp peaks. The green (blue) region is the spatial extent of the PL peak labelled QD1F1 (QD2F1) in relation to the region where the X^0 PL reduces to half of its maximum value (area enclosed by the black contour). Red region depicts the spatial extent of sharp peak located close to the edge of the flake which has reduced overlap with X^0 region. (Left panel) High resolution PL spectra of QD1F1 and QD1F2 showing extremely narrow linewidths.

Figure 2: Photon correlations and photoluminescence lifetimes of quantum dots a, Second order photon correlation function ($g^2(\tau)$) of photoluminescence (PL) measured using Hanbury-Brown-Twiss setup shows pronounced dip (antibunching) at zero time delay for the emission lines QD1F1 (left panel) and QD4F1 (right panel), confirming that they originate from zero-dimensional emitters - quantum dots. **b,** Time-resolved PL of QD1F1 (left panel) and QD3F1 (right panel) measured using pulsed Ti:Sapphire laser of ~ 5 ps shows long lifetime of the excited state typical of zero-dimensional emitters.

Figure 3: Stability of emission and spectral wandering of quantum dots. a, Waiting time distribution of photoluminescence (PL) from QD1F1 as function of time delay between successive single photon detection events shows single exponential decay, indicating absence of intensity intermittency on timescales larger than the average time for photon detection, τ_{det}. **b,** (Left panel) Time-trace of PL emission of a typical quantum dot (QD) measured with low spectral resolution shows stable peak position. (Right panel) High resolution PL time-trace of another

QD showing spectral wandering with a range of 1 meV. The synchronized wandering of the two peaks, strongly suggests that they arise from the same QD and are associated with electron-hole exchange split exciton transitions.

Figure 4: Magnetic field dependence of quantum dot photoluminescence. a, (Left panel) Polarisation resolved magnetic field (B) dependence of photoluminescence (PL) from a quantum dot (QD1F2) in perpendicular B (Faraday geometry) shows splitting of the two peaks with increasing B. The PL is detected in a circularly polarised basis (σ_1). Even though the high energy peak should be dominant at higher B because of its emission helicity being that of the detection basis, efficient thermal relaxation causes the low energy peak to be stronger. In the opposite detection basis (σ_2), (see Fig. 4b), the low energy peak is even stronger for $B > 0$. (Right panel) B parallel to the sample (Voigt geometry) does not show any measurable splitting. **b,** The helicity of polarisation of the two split peaks of quantum dot QD2F1 denoted by red and blue traces switches sign upon reversal of the direction of B. **c,** Extracted splitting between the two peaks in Faraday geometry of QD2F1 (left panel) and QD1F2 (right panel) as a function of B is fitted with a hyperbolic function (see text) to extract the magnetic moment and the zero-field exchange splitting.

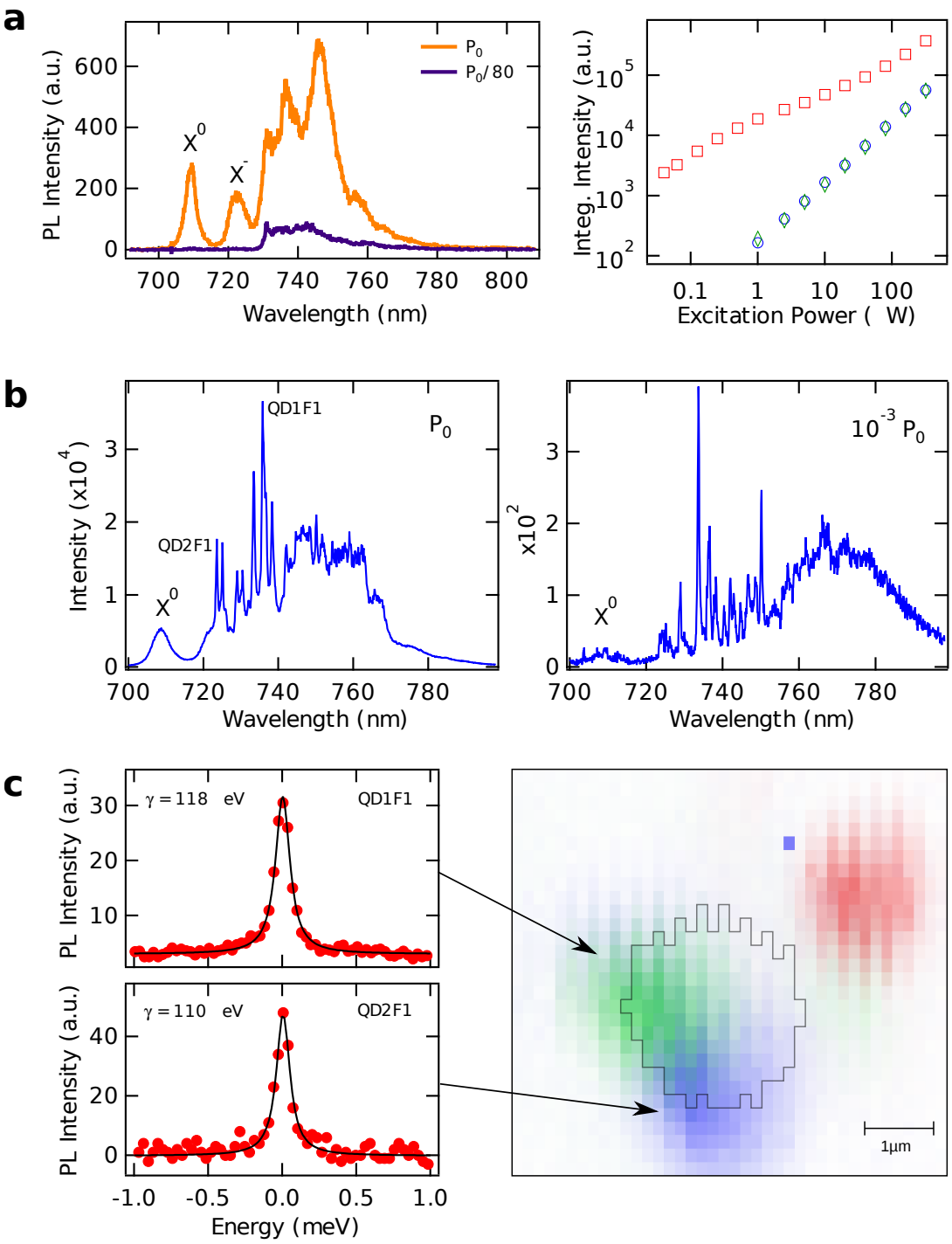
a
PL Intensity (a.u.)
600
400
200
0
700
720
740
760
780
800
Wavelength (nm)
X0
X-
P0
P0/80
Integ. Intensity (a.u.)
10^5
10^4
10^3
10^2
0.1
1
10
100
Excitation Power (W)
b
Intensity (x10^4)
3
2
1
0
700
720
740
760
780
Wavelength (nm)
QD1F1
QD2F1
X0
P0
x10^2
10^-3 P0
c
PL Intensity (a.u.)
30
20
10
γ = 118 eV
QD1F1
40
γ = 110 eV
QD2F1
-1.0
-0.5
0.0
0.5
1.0
Energy (meV)
1μm

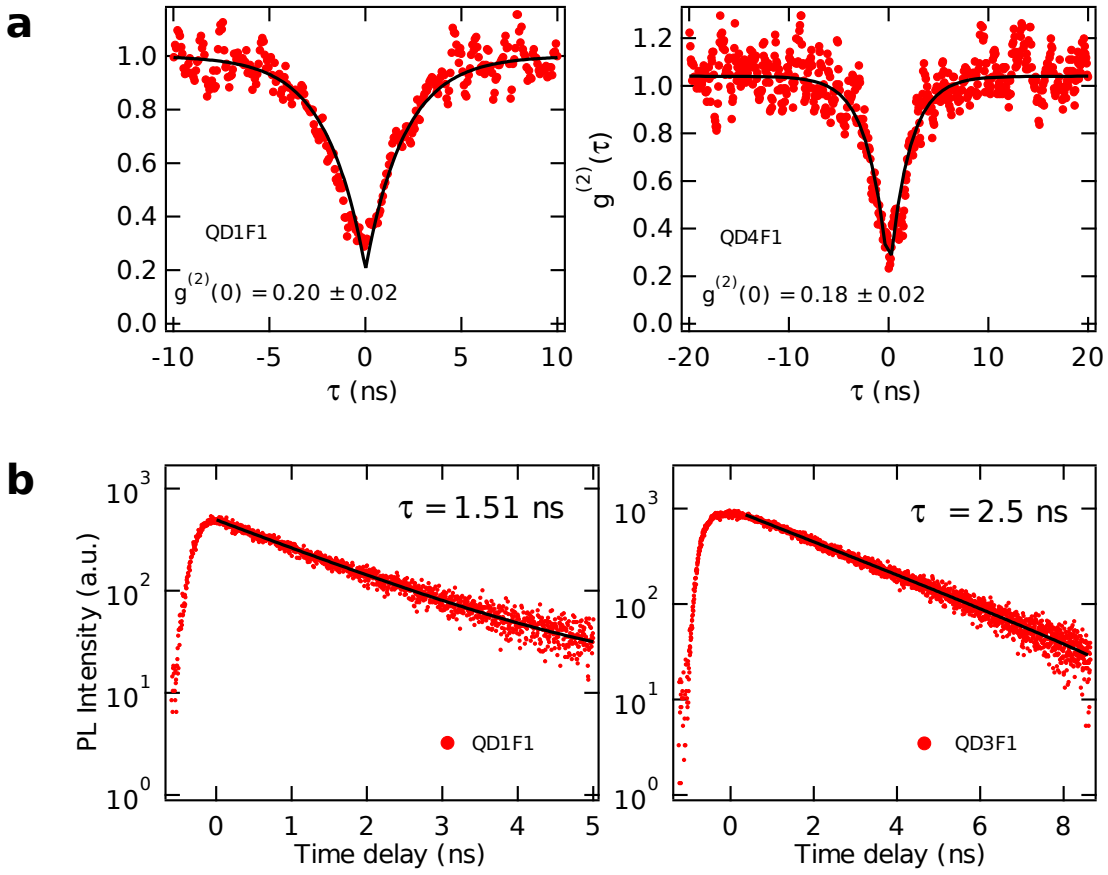
a
QD1F1
g(2)(0) = 0.20 ± 0.02
τ (ns)
QD4F1
g(2)(0) = 0.18 ± 0.02
g(2)(τ)
τ (ns)
b
τ = 1.51 ns
QD1F1
PL Intensity (a.u.)
Time delay (ns)
τ = 2.5 ns
QD3F1
Time delay (ns)

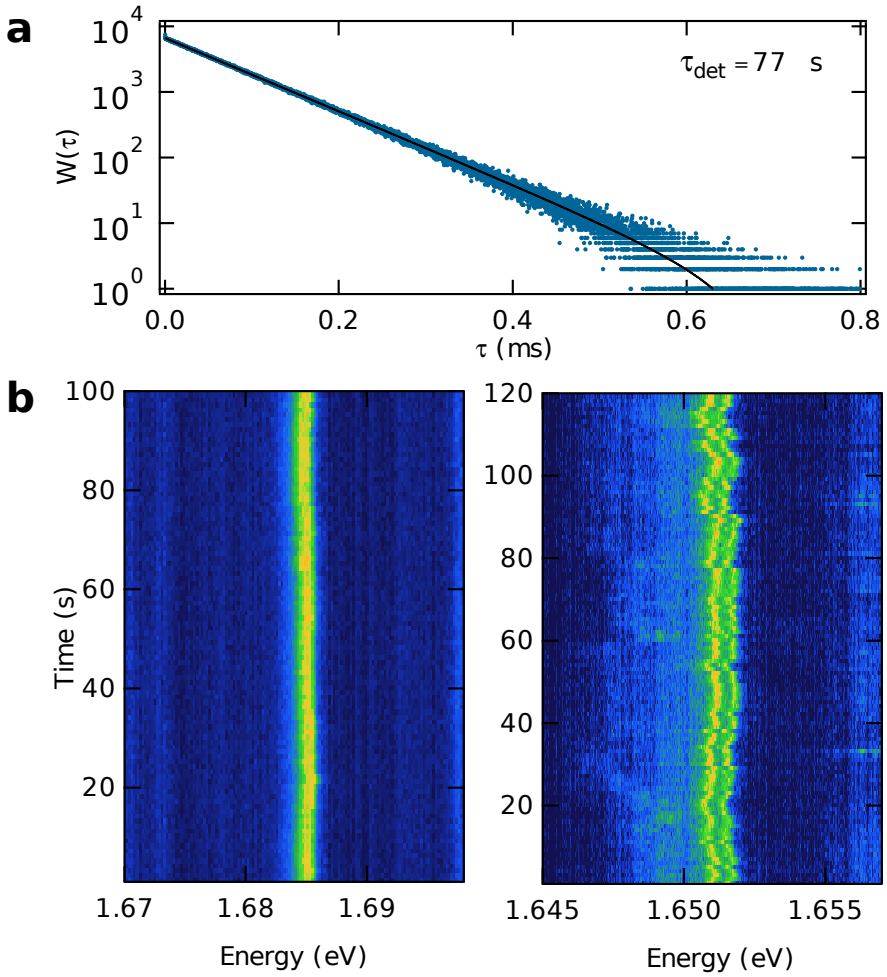
a
10^4
10^3
10^2
10^1
10^0
W(τ)
$\tau_{det} = 77$ s
0.0
0.2
0.4
0.6
0.8
τ (ms)
b
100
80
60
40
20
Time (s)
1.67
1.68
1.69
Energy (eV)
120
100
80
60
40
20
1.645
1.650
1.655
Energy (eV)

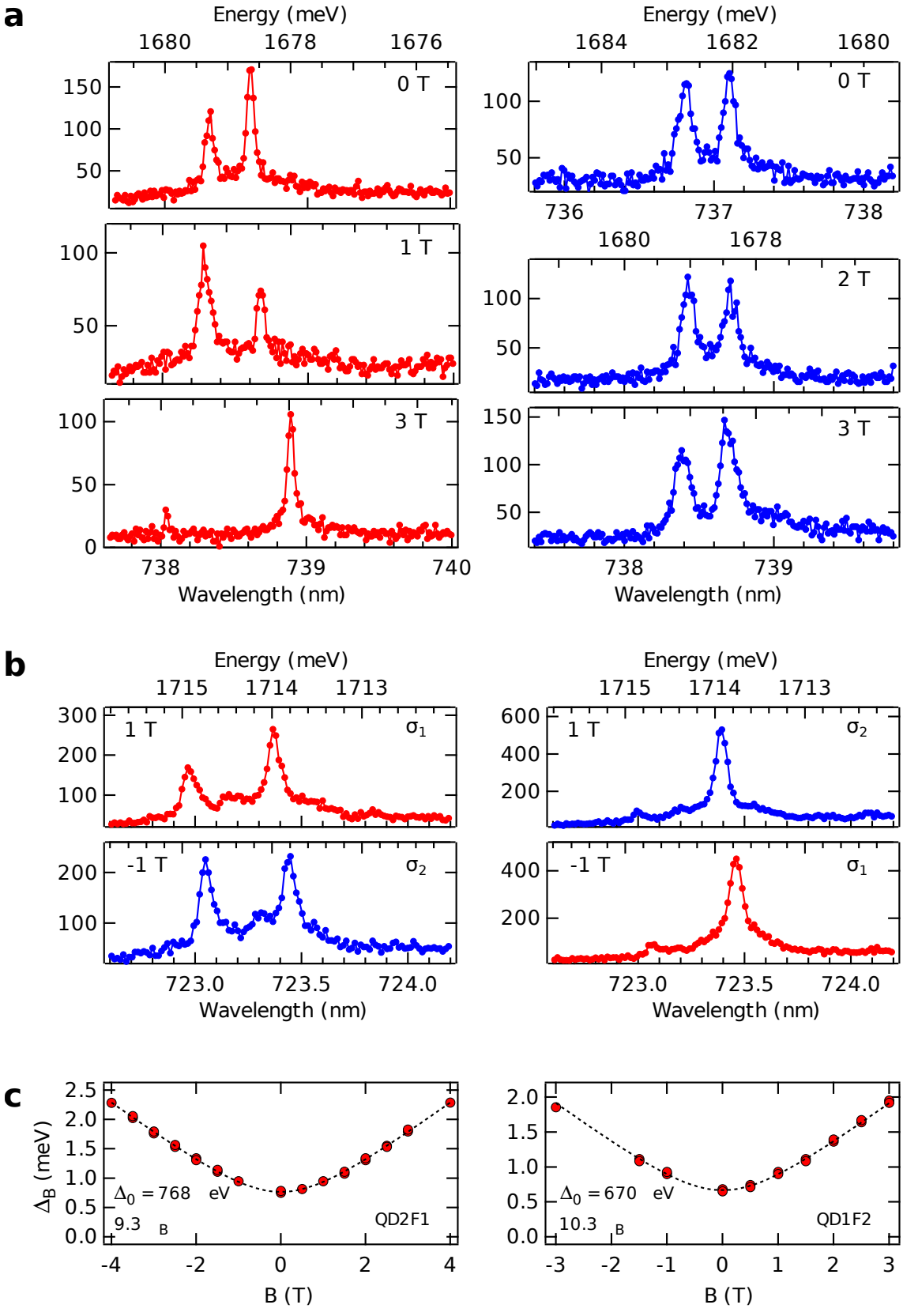
a
Energy (meV)
1680
1678
1676
0 T
1 T
3 T
150
100
50
0
738
739
740
Wavelength (nm)
Energy (meV)
1684
1682
1680
0 T
2 T
3 T
736
737
738
1680
1678
738
739
Wavelength (nm)
b
Energy (meV)
1715
1714
1713
1 T
-1 T
σ1
σ2
300
200
100
723.0
723.5
724.0
Wavelength (nm)
Energy (meV)
1715
1714
1713
1 T
-1 T
σ2
σ1
600
400
200
723.0
723.5
724.0
Wavelength (nm)
c
ΔB (meV)
Δ0 = 768 eV
9.3 B
QD2F1
2.5
2.0
1.5
1.0
0.5
0.0
-4
-2
0
2
4
B (T)
Δ0 = 670 eV
10.3 B
QD1F2
-3
-2
-1
0
1
2
3
B (T)

Supplementary Information:

Figure S1: (Left panel) Normalized photoluminescence spectra of flake0 for different incident laser powers. The different PL traces for exciton and trion emission overlap with each other after normalizing with the incident laser power implying a linear dependence of PL on incident laser power. No broadening of the exciton and trion peak is observed even for the highest incident power of ~ 320 μW. (Right panel) The impurity band emission, normalised with the incident laser power, exhibits saturation (sub-linear dependence) and drastic changes in the spectral features with increasing laser power.

Figure S2: Photoluminescence excitation (PLE) spectroscopy of quantum dots QD3F1 and QD1F2 performed by scanning a continuous wave tunable Ti:Sapphire laser near the free exciton resonance. Total integrated photoluminescence (PL) counts are plotted against laser wavelength showing clear enhancement of PL intensity at free exciton resonance (708 nm) for QD3F1. QD1F2 shows a similar enhancement however, at a slightly red-shifted wavelength.

Figure S3: Magnetic field dependent splittings in the Faraday geometry for a few different dots with hyperbolic fits (see main text) to extract the magnetic moment and the exchange splitting at zero magnetic field.

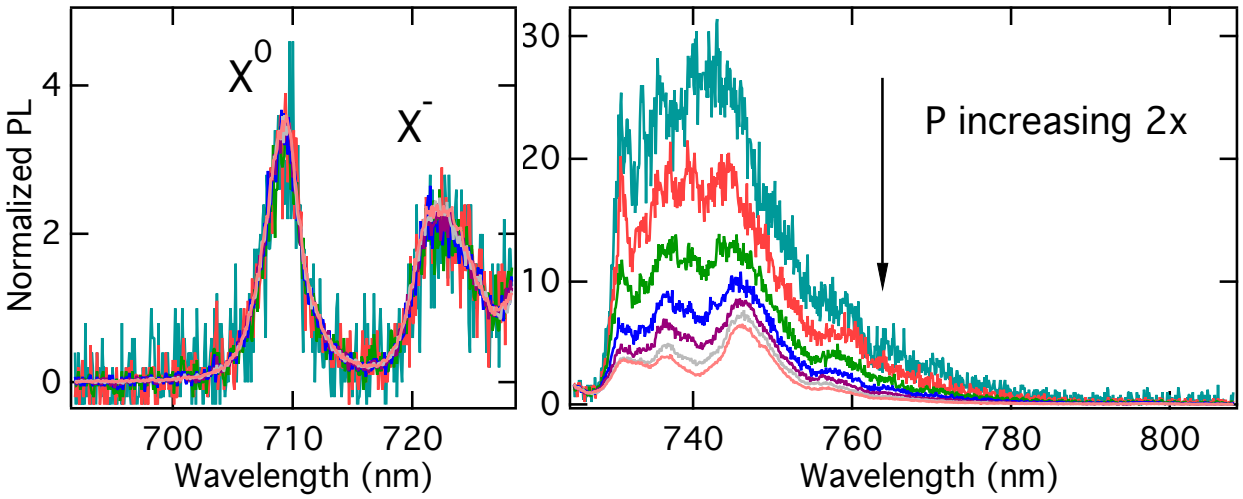
Normalized PL
X0
X-
0
2
4
700
710
720
Wavelength (nm)
0
10
20
30
740
760
780
800
Wavelength (nm)
P increasing 2x

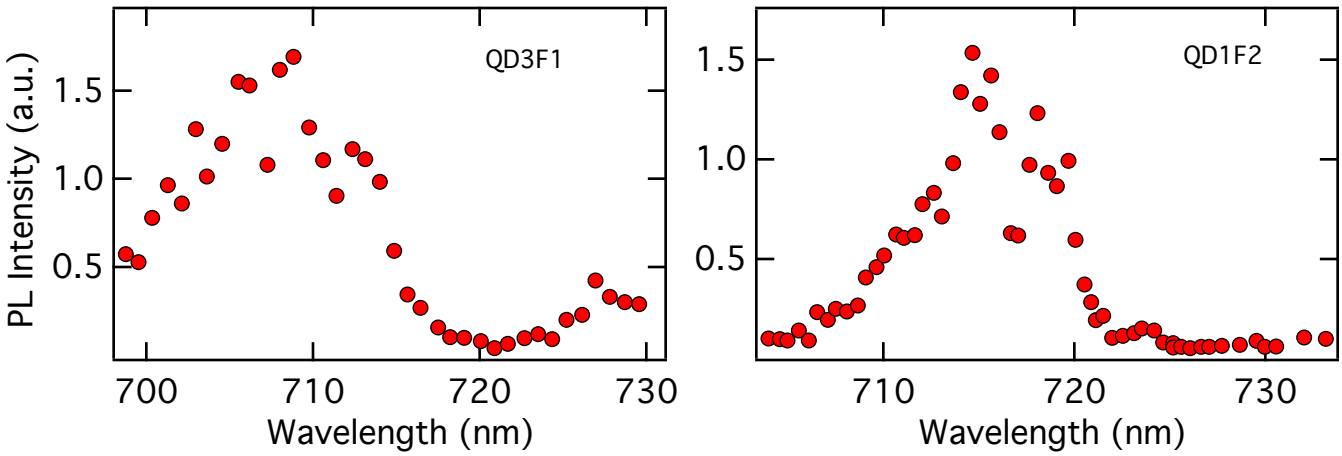
QD3F1
PL Intensity (a.u.)
1.5
1.0
0.5
700
710
720
730
Wavelength (nm)
QD1F2
1.5
1.0
0.5
710
720
730
Wavelength (nm)

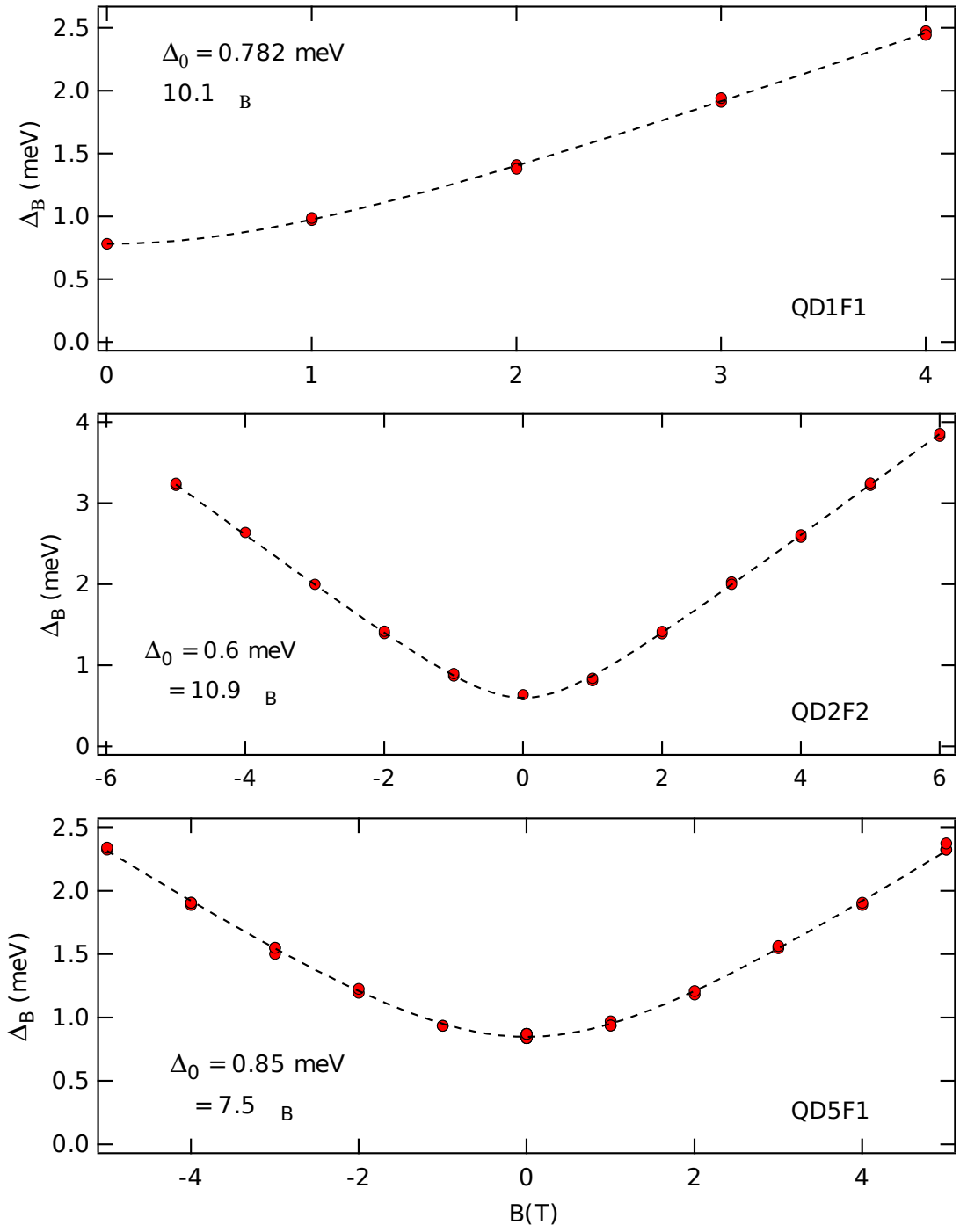
$\Delta_0 = 0.782$ meV
10.1 B
QD1F1
Δ_B (meV)
$\Delta_0 = 0.6$ meV
= 10.9 B
QD2F2
$\Delta_0 = 0.85$ meV
= 7.5 B
QD5F1
B(T)